Estuarine, Coastal and Shelf Science 276 (2022) 108032

Contents lists available at ScienceDirect

Estuarine, Coastal and Shelf Science

journal homepage: www.elsevier.com/locate/ecss

Impacts of bioturbation on iron biogeochemistry and microbial communities in coastal sediment mesocosms under varying degrees of hypoxia

Jacob P. Beam [a,1], Alexander B. Michaud [a,1], David T. Johnston [b], Peter R. Girguis [c], David Emerson [a,*]

[a] Bigelow Laboratory for Ocean Sciences, East Boothbay, ME, USA
[b] Department of Earth and Planetary Sciences, Harvard University Cambridge, MA, USA
[c] Department of Organismic and Evolutionary Biology, Harvard University Cambridge, MA, USA

ARTICLE INFO

Keywords:
Bioturbation
Iron cycling
Hypoxia
Intertidal sediments

ABSTRACT

Coastal sediments are important sources of dissolved iron (dFe) that make the coastal ocean iron replete, and contribute an important supply of dFe to the photic regions of the adjacent open ocean. The biogeochemical processes that dictate sedimentary dFe flux are a complex interplay of microbial activities related to reduction-oxidation condition, Fe and S cycling, and sediment bio-mixing and bio-irrigation by benthic fauna. We investigated the effect of bottom water oxygen concentration on iron dynamics in laboratory mesocosms in the presence and absence of the common polychaete *Nereis diversicolor*. Mesocosms were established using sediment obtained from a local intertidal mudflat, maintained with varying levels of hypoxia (defined as <63 μM dissolved O_2), and monitored for changes in iron biogeochemistry. At the end of the experiment, subcores were taken to measure solid phase Fe species and microbial community analysis via 16S rDNA gene sequencing. Bioturbation played an important role in increasing the quantity of poorly crystalline Fe(III)-oxides within the sediments, but decreasing the flux of Fe(II) across the sediment-water interface. These results further demonstrate the importance of bioturbation for sedimentary Fe-cycling and show a complex response to hypoxia involving both animal behavior and microbial response.

1. Introduction

Iron is an essential element for life. Its scarcity in one-third of ocean surface waters can result in limiting light-driven primary productivity by phytoplankton (Martin et al., 1990; Tagliabue et al., 2017). Supply of iron, primarily in the form of dissolved iron (dFe), to coastal areas is sourced from coastal shelf sediments and riverine terrestrial inputs (Laufer-Meiser et al., 2021; Raiswell and Canfield, 2012). Some fraction of this dFe is carried offshore, in what is often referred to as the shelf to basin iron shuttle, which provides iron to both deep water and the open ocean photic zone (Elrod et al., 2004). In the photic zone, it helps alleviate iron limitation in phytoplankton (Lenstra et al., 2019; Severmann et al., 2010). There is ongoing debate as to how much coastal sediment derived dFe may contribute globally to iron inventories in the open ocean (Birchill et al., 2019); therefore, it is important to determine and quantify mechanisms of dFe release from nearshore sediments.

The majority of important biogeochemical transformations of iron that impact both its abundance and availability in the water column occur in shallow surficial marine sediments. Primary controls on sedimentary iron cycling include the activity of resident Fe- and S-cycling microorganisms, the amount of labile organic carbon in sediments, bottom water oxygen concentration of the overlaying water, and the activity of sediment dwelling macro- and meiofauna that actively bio-irrigate and/or biomix the upper sediment layers in a process we will refer to as bioturbation (Aller and Cochran, 2019; Beam et al., 2020; Butterfield, 2018; Herbert et al., 2022; Meysman et al., 2006b; van de Velde et al., 2020). A primary outcome from the activity of burrowing benthic fauna is to increase the surface area of sediment-water interfaces (Davey, 1994), thus providing a larger area for redox transitions of Fe that ultimately control its fate (Gribsholt et al., 2003; Meysman et al.,

* Corresponding author. Bigelow Laboratory for Ocean Sciences, 60 Bigelow Dr, East Boothbay, ME, 04544, USA.
E-mail address: demerson@bigelow.org (D. Emerson).
[1] These authors contributed equally to this work.

https://doi.org/10.1016/j.ecss.2022.108032
Received 12 December 2021; Received in revised form 27 July 2022; Accepted 12 August 2022
Available online 23 August 2022

2006a). Animal burrowing also stimulates a diverse group of lithotrophic Fe- and S-cycling microorganisms that inhabit sediment redox boundaries and drive sedimentary iron dynamics along with chemical processes linked to the products of microbial metabolisms (Beam et al., 2018; Buongiorno et al., 2019; Laufer et al., 2016; Michaud et al., 2020; Otte et al., 2019). It is the combined activity of microbes and benthic fauna that exert primary control on the flux of dFe from the sediment to the ocean water column; yet there are few studies that have specifically attempted to link benthic processing events with microbial populations and degree of hypoxia.

The aforementioned studies establish the importance of coastal watersheds in dFe flux to the ocean. Ocean warming directly reduces the solubility of O_2 in water, increases water column stratification which restricts oxygen supply to deeper waters, and excessive nutrient inputs from river run-off coupled with regional ocean basin topography leads to bottom water hypoxia (Fennel and Testa, 2019). Today, continued ocean warming coupled with further anthropogenic nutrient loading will expand hypoxic and anoxic regions, and alter coastal sedimentary iron biogeochemistry and iron fluxes (Bianchi et al., 2021). Our definition of hypoxia is equivalent to that used in other marine sediment studies where hypoxia is < 63 μM and anoxia is less than the detection limit of our method of ~0.1 mM dissolved O_2 in the water (Jessen et al., 2017). In purely chemical terms, bottom water hypoxia and anoxia will reduce the rate of O_2-dependent Fe(II) oxidation leading to increased Fe (II) diffusing from sediments into the water column (Elrod et al., 2004). However, hypoxic conditions may kill or alter the behavior of bioturbating macrofauna, thus decreasing sediment-water interface surface area for iron cycling. It is well-established that bioturbation impacts sedimentary Fe and S biogeochemistry, with most evidence suggesting bioturbation increases mobilization of dFe (van de Velde and Meysman, 2016). However, interactions between hypoxia, bioturbation, and dFe mobilization are further complicated by the adaptive response of marine worms to increased rates of bioirrigation in response to hypoxia. Increased rates of burrow flushing may facilitate the transport of more Fe(II), and result in more dFe, moving from the sediments to the water column (Elrod et al., 2004; Herbert et al., 2021; van de Velde et al., 2021). Anthropogenic and/or climate change-caused declines in coastal dissolved oxygen—hypoxia and anoxia—will potentially have a negative impact on dFe release by retaining and burying the majority of iron in marine sediments as iron sulfides. Thus, it is important to understand the impact lower oxygen conditions will have on the sedimentary Fe cycle and dFe flux under controlled laboratory conditions.

The flux of dFe from coastal shelf sediments is estimated to be 72 Gmol Fe yr^{-1} (Dale et al., 2015). The highest specific fluxes were measured using benthic flux chambers in hypoxic regions with < 80 μmol $O_2 \cdot m^{-2} \cdot day^{-1}$ and significant bioturbation (Homoky et al., 2012). Measurements with benthic chambers are important to understanding Fe fluxes under various bottom water O_2 regimes; however, laboratory mesocosms allow for greater control to understand faunal, microbial, and biogeochemical responses to specific environmental perturbation. We conducted mesocosm experiments with sieved sediment from an intertidal mudflat, and compared paired aquaria, with a marine polychaete present or absent, under four different controlled dissolved oxygen concentrations to simulate different bottom water oxic conditions. In each experiment, we quantified dFe flux into the overlying water, solid-phase Fe and S in the sediments, and characterize microbial community composition. The resulting data illustrate the role of bioturbation on Fe dynamics and microbial community composition under different oxygen regimes that simulate increasing hypoxia.

2. Material and methods

2.1. Mesocosm setup

The aquaria mesocosms used for these experiments were custom fabricated from polycarbonate (0.31 cm wall thickness; dimensions of 30 cm × 15 cm x 25 cm; $V = 1.125 \times 10^{-2}$ m^3). Coastal sediments were harvested on four separate occasions: October 2017 for $O_2 = 10$ μmol L^{-1} (extreme hypoxia); May and November 2017, for $O_2 = 280$ (fully oxic) and 48 μmol L^{-1} (high hypoxia), respectively, and June 2018 for $O_2 = 106$ μmol L^{-1} (intermediate oxic). All sediments were collected from approximately the same location in an intertidal mudflat ("The Eddy", Sheepscot River, Maine, USA, latitude 43.9948, longitude −69.6486, salinity = 30–35‰) from the upper 20–25 cm of sediment. Collected sediments were returned to the laboratory and, within 1 h, were progressively sieved through 1 mm and 0.4 mm mesh screens to remove large macrofauna and detrital material (e.g., sticks, leaves, and stones). The sieved sediments were placed in the mesocosms to an approximate depth of 15 cm and sand-filtered, autoclaved seawater was added to make a 10 cm deep water column above the sediment. The sediments were allowed to settle for ~24 h before starting the experiment, which was initiated (day = 0) upon introduction of worms to the experimental aquarium. Sets of two aquaria each, one with worms and one without, were incubated for 10 days under continuous aeration. In total, four experiments were set up as described above with their overlying dissolved O_2 concentrations manipulated to 10, 48, 106 and 280 μmol L^{-1} to mimic hypoxia to saturated conditions. *Nereis* (*Hediste*) *diversicolor* (25 individuals per tank, equivalent to 500 individuals m^{-2}) were collected from the same field site, and added back to the bioturbated aquaria, while the control aquaria contained no animals. *N. diversicolor* was the most abundant polychaete in these sediments. This worm number was at the lower end of natural population abundances (Davey, 1994; Kristensen and Kostka, 2013). Worms were collected as discovered in the field with no visual bias towards larger or small individuals; *N. diversicolor* individuals that were greenish in color were not selected, since this coloration indicates they are in the process of sexual reproduction (Bartels-Hardege and Zeeck, 1990). Animals were returned to the field after the experiments ended. Oxygen in the mesocosms was continuously monitored with an O_2 sensor spot and optical flourometer (Pyro Science GmbH, Germany) every minute for 10 days with the temperature compensation probe placed in the overlying water next to the sensor spot. The aquaria remained at ambient room temperature (~19–20 °C) and were covered with a box, except for sampling periods, to limit light exposure.

2.2. Imaging

Photographs of each mesocosm were taken once during every 24-h sampling period, starting at day 1, after the sediment was fully settled. Images were cropped to include only the sediment and approximately 2 cm of overlaying water. The cropped images were edited with Apple Photos (version 5.0) to adjust exposure, as well as improve contrast and sharpness, to maximize visualization of worm burrows that were visible through the walls of the mesocosm along with sediment color changes associated with burrows. Worm burrow walls that had an orange layer of iron oxides associated with them were hand traced using ImageJ software (Schneider et al., 2012), and used to calculate an area of burrow walls. From these same images, cross-section diameters of the visible, hollow worm burrows were also measured.

2.3. Porewater ferrous iron analysis

Rhizon samplers (10 cm long filter with 0.12–0.18 μm pore size; Rhizosphere Research Products, Wageningen, Netherlands) were glued into the aquarium walls at 3 cm depth intervals and were used to remove porewaters from sediments with a 10 mL syringe every 24 h to measure aqueous dissolved Fe(II) (dFe). The porewaters (~1.5 mL) were dispensed into a 1.5- or 2-mL centrifuge tubes and 0.25 mL was immediately pipetted into ferrozine solution to measure ferrous iron (Stookey, 1970). Absorbance was measured on a Thermo-Fisher spectrophotometric plate reader at 540 nm from 0.5 mL samples via Ferrozine method (Stookey, 1970). Timecourse figures were produced by linear

interpolation between the sampled depths and dates. To better approximate the ferrous iron concentration around the sediment-water interface, we assumed a consistent diffusive boundary layer (DBL) of 500 μm thickness and a homogenous water column above the DBL. We make these assumptions because the ferrous iron concentrations in the water column above the sediments was always below detection limit and mixed due to aeration (Fig. 4, Jørgensen and Des Marais, 1990). The flux of ferrous iron across the sediment-water interface was calculated using the concentration gradient between the top of the DBL and the first measured porewater ferrous iron concentration. The diffusion coefficient for ferrous iron at 18 °C is 5.43×10^3 cm^2 s^{-1} (Broecker and Peng, 1974) and the porosity was assumed to be 0.85.

2.4. Poorly-crystalline iron oxide analysis

Sediment sub-cores (n = 3) were sampled from both the bioturbated and control aquaria after the 10-day incubation period using a cut-off 60 mL syringe, and immediately frozen in liquid nitrogen or frozen at −80 °C. The sub-core samples were split in half with a sterile razor blade and were sliced into 1 cm sections up to 10 cm depth in a glove bag under a N_2/H_2 atmosphere. Sedimentary poorly-crystalline iron oxides (i.e., ferrihydrite and lepidocrocite) were extracted using hydroxylamine hydrochloride for 48 h under anoxic condition (Poulton and Canfield, 2005). The poorly-crystalline iron oxide extractions were diluted 1:100 and mixed with Ferrozine buffer and the absorbance measured using the plate reader as described above. The amount of poorly-crystalline iron oxides were integrated over the top 10 cm, in 1-cm intervals, across three replicate cores from each mesocosm and treatment.

2.5. Acid volatile sulfide analysis

The other half of the split sub-cores from the aquaria were re-frozen and shipped on dry ice for acid volatile sulfide (AVS) analysis at McGill University (Montreal, Quebec). The sediment was placed in a sealed reaction flask and 6 M HCl was added to the reaction flask through a side port. The acid and sediment were allowed to react under N_2 flow and the released sulfide was passed through a 0.1 M citrate buffer, then trapped in 5 mL of 5% Zinc Acetate solution (Fossing and Jørgensen, 1989; Røy et al., 2014). The precipitated ZnS was quantified colorimetrically using the Cline assay (Cline, 1969). AVS was integrated over the top 7 cm of sediment depth across three replicate cores, as this was the deepest depth analyzed across all mesocosms and experiments.

2.6. DNA extraction, 16S rDNA gene sequencing, and analysis

A sub-sample of the same sediment sub-cores, described above, was used for DNA extraction, except that DNA samples were only taken at 1, 3, 5, and 10 cm depth intervals. To reiterate, for each bioturbated mesocosm, triplicate DNA samples were obtained, while a single set was obtained for each control; the rationale being that bioturbated mesocosms would likely exhibit more variability than the unperturbed controls, and sequencing costs were resource limited. DNA was extracted using a Qiagen DNA Power Soil Extraction kit following the manufacturers protocol with a modification in Step 1 that involved the removal of 200 μL of extraction buffer from the bead-beating tubes and replacing it with 200 μL of molecular grade 25:24:1 phenol:chloroform:isoamyl alcohol (Millipore Sigma). Our previous work had shown this improved DNA yields, especially from Fe(III)-oxides in sediments (Scott et al., 2017). The DNA at the final elution step was eluted with 100 μL of molecular grade DNase-free water. The samples were frozen at −20 °C until further processing.

The 16S rDNA gene was amplified using V4–V5 primers 515F/926R at the Integrated Microbiome Resource (Dalhousie University, Halifax, Nova Scotia, Canada). Paired end reads were assembled and classified using a mothur (Schloss et al., 2009) pipeline from the mothur MiSeq standard operating procedure (Kozich et al., 2013). Assembled sequences that contained ambiguous bases, homopolymers greater than 8 nucleotides, or were 5 nucleotides shorter or longer than the sequence length predicted based on these primers were removed from the analysis. Reads were subsampled so each sample had the same number of reads for OTU clustering and classification. For our primary analysis, operational taxonomic units (OTUs) were clustered at 85%, which corresponds roughly to the class-order taxonomic level (Yarza et al., 2014) and was chosen for comparative analysis to limit the number of clusters generated for comparisons and lend clarity to data representations. It also allowed direct comparison with our previous seasonal analysis of sediments collected from the same site (Beam et al., 2020). This process yielded a total of 12,437 unique OTUs from all the experiments. Relative abundances, based on OTU counts, were utilized to build a heatmap in RStudio (R Core Team, 2020) of the top OTUs that were greater than 0.5% abundance in any one sample.

2.7. Ecostates

An ecostate clustering model (Record et al., 2017) was used to compare the overall microbial communities from different mesocosm treatments to one another, and to a set of sediment samples from the Eddy, the site of initial intertidal mud for experiments. Each ecostate represents a consortium of taxa that clusters together consistently throughout the sampling program, as well as the respective relative abundances of taxa (O'Brien et al., 2016). For this analysis, samples were clustered at 85% identity level using average linkage hierarchical clustering of the Bray-Curtis dissimilarity as implemented in the R package vegan (Oksanen et al., 2013). Ecostates were then numbered and color coded and mapped back to the OTU-based heatmap (R Core Team, 2020).

2.8. Data availability

All 16S rDNA gene sequencing reads can be found under the NCBI Bioproject PRJEB37656. All mesocosm geochemical data is located in Supplemental Data File 1. The code used to process sequence data and geochemical data is accessible on a github repository (https://github.com/abmichaud/eddy).

3. Results and discussion

3.1. Mesocosm performance

A total of four mesocosm experiments were set up with O_2 concentrations in the overlaying water set at 10, 48, 106, and 280 μM to simulate bottom water oxic conditions ranging from extreme hypoxia to 100% oxygen saturation. In each case the overlaying water equilibrated at the appropriate O_2 concentration for 24h, before *Nereis diversicolor* worms were added back to the bioturbated tank, while the other tank served as a nonbioturbated control. All tanks maintained nearly constant O_2 levels during the course of an experiment (Supplemental Fig. 1). The extreme hypoxic experiment (10 μM O_2) resulted in all the worms remaining on the sediment surface with significant mortality, and the experiment was ended within 48 h. Experimental studies have indicated *N. diversicolor* tolerated up to 72 h of complete anaerobiosis under purely aqueous conditions (Schöttler, 1979); however, in our mesocosms, these worms exhibited minimal tolerance to this level of hypoxia. It is possible the additional respiration required for burrowing caused a reduced tolerance to anaerobiosis for *N. diversicolor* in the mesocosms; alternatively, the transition from oxic to extreme hypoxic conditions may have been too great a shock for these animals to acclimate.

The visual results of the other three experiments are shown in Fig. 1 and Supplementary Figs. 2 and 3. In these trials, all the worms began burrowing within 24 h of addition to the sediment, and there was no observed mortality during the 10 d experiment. The visual appearance

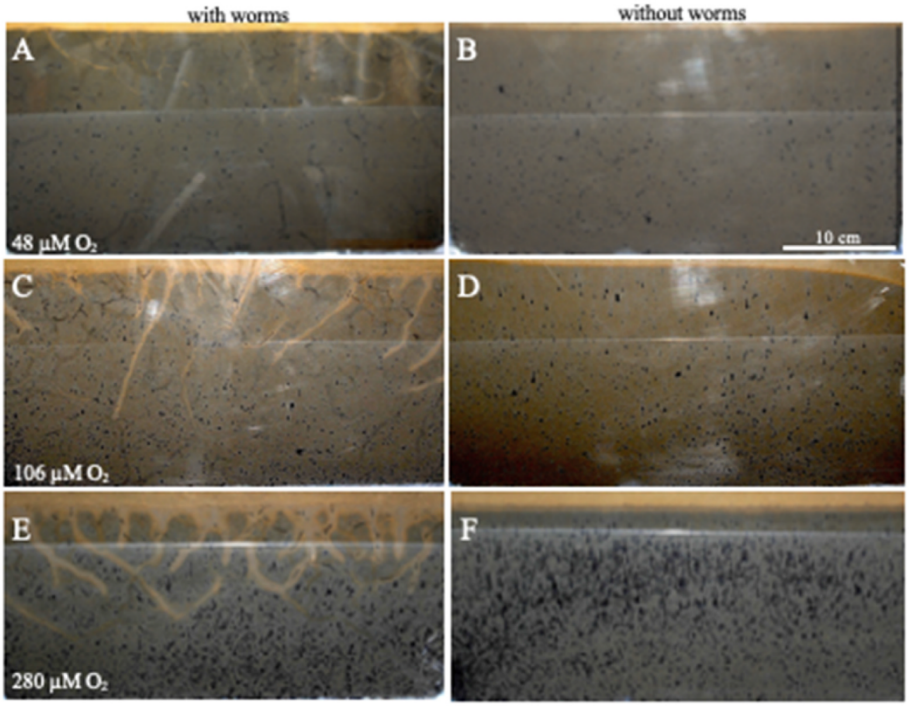

Fig. 1. Comparison of mesocosms at different O_2 levels, with (A, C, E) and without (B, D, F) *Nereis diversicolor*. Each image pair was taken on day 10 of the given experiment. Note the increase in FeOOH associated with burrow walls with increasing O_2 concentration. The white streaking is due to reflectance of light off the polycarbonate walls of the mesocosms.

of worm burrows against the transparent tank wall was used as a proxy for worm burrowing behavior for each experiment (Fig. 1, Supplemental Figs. 2 and 3). Previous studies suggest that worms burrowing against a glass aquaria wall may reduce 'burrowing effort' by 10% (Dorgan et al., 2005), thus there may be some bias towards burrows being associated with the polycarbonate aquaria walls. However, top-down visualization of burrow holes in the aquaria at the end of each experiment revealed an apparent random distribution of holes across the sediment surface (data not shown), suggesting there was not a strong bias toward burrowing behavior along the mesocosm walls. It is apparent that *N. diversicolor* burrows were coated with progressively more Fe(III)-oxides with increasing O_2 concentration in the overlaying water (Figs. 1 and 2 and Supplemental Fig. 2). *N. diversicolor* burrowing activity was followed during each experiment, and showed increased burrow number and depth at 280 μM O_2 at day 1 or day 2 compared to the lower O_2 treatments, with progressively less activity at 106 μM and 48 μM O_2 treatments (Supplemental Fig. 2 and Table 1). Somewhat counter-intuitively, by day 5, burrows were observed at the deepest depths (15 cm) in the two lower O_2 aquaria, but burrows were not observed below approximately 10 cm in the fully oxygenated aquaria (Supplemental Fig. 2). An image-based analysis of the Fe(III)-oxide coatings surrounding clearly visible burrows showed that these coatings initiated sooner, and were thicker under more oxic conditions, Fig. 2 and Table 1. For the 280 μM O_2 treatment, it appeared burrows closer to the surface had increased areas of oxidation compared to the deeper burrow walls (Fig. 2); whereas under the more hypoxic conditions, the oxidation zones were more consistent with depth, but the total area of oxidation was less, especially for the 48 μM O_2 treatment.

We are not aware of other sediment mesocosm studies that have purposefully exposed *N. diversicolor* to varying levels of hypoxia. Detailed measurements around *N. diversicolor* burrow walls have shown that under fully oxic conditions, the O_2 concentration around burrow walls ranges from 25 to 50% of that of the overlaying water, and that O_2 penetrates 2–3 mm perpendicular to the burrow wall (Pischedda et al., 2012). This is consistent with our observed results with visible Fe

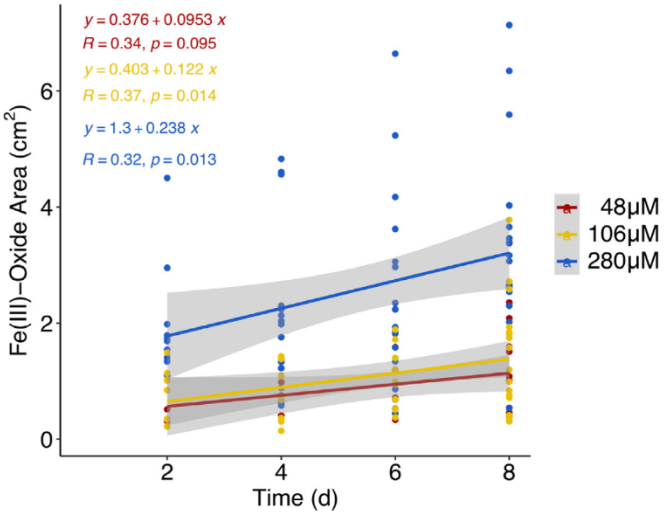

Fig. 2. Bar graph showing increase in total area of Fe(III)-oxides surrounding worm burrow walls in the mesocosms incubated under 48, 106, and 280 μM dissolved oxygen levels over time (See methods). On Day 2, oxides were only visible in mesocosm with 280 μM O_2. These data were produced by outlining the visible burrow walls through the clear mesocosm walls with apparent rust-colored oxides as depicted in Fig. 1 and Supplementary Fig. 2.

(III)-oxide presence at approximately 2 mm from the burrow wall into the sediment (Table 1). An analysis of bioturbated North Sea sediments showed that when the O_2 concentration of overlaying seawater was reduced to 25% of saturation, advective water flux increased at least 3 times compared to fluxes in animal burrows under fully oxygenated conditions (Forster et al., 1995). From these studies, it is reasonable to assume that reduction of O_2 concentrations in the overlaying water led to higher ventilation rates by *N. diversicolor* in our microcosms. Despite these presumed higher burrow ventilation rates in waters with lower

Table 1
Measurements of the burrow diameters, including the surrounding rust-colored layers on day 5 and 9 for the three dissolved oxygen treatments. Each value is the average of 12 separate measurements of representative burrows from each mesocosm and the standard deviation is shown in parentheses. The burrow alone value is the average of 12 measurements of burrow wall diameters without any surrounding Fe(III)-oxides.

O_2 concentration (μM)	48		106		280		Burrow alone
Time (d)	5	9	5	9	5	9	
Burrow Width (mm) (Std. Dev.)	1.41 (0.62)	1.61 (0.55)	1.71 (0.48)	3.25 (0.6)	3.17 (1.01)	5.55 (1.58)	1.32 (0.30)

dissolved oxygen concentrations, the accumulation of Fe(III)-oxides surrounding burrow walls was still greatest in the highest O_2 treatment aquaria (Fig. 2 and Table 1). This indicates there was a greater potential for Fe(II) to be transported via ventilation from the sediment under hypoxic conditions, rather than being oxidized within the burrows, which would support the hypothesis that hypoxic water columns foster conditions for more dFe to be released from burrows.

3.2. Iron biogeochemistry

The porewater profiles of Fe(II) in all three bioturbated and control aquaria follow similar trends regardless of the oxygen concentration. In the aquaria containing *N. diversicolor*, porewater Fe(II) concentrations were more variable over time, and overall lower in near-surface sediment compared to equivalent depths in the paired, nonbioturbated aquaria (Fig. 4). These observations imply that bioturbation pushes the peak pore water Fe(II) concentration deeper into the sediments (Fig. 4). Thus, bioturbated mesocosms had fluxes of below detection, 13 ± 2.7, and 18 ± 1.8 μmol Fe^{2+} cm^{-2} d^{-1} across the sediment-water interface for the 280, 106, and 48 μM O_2 mesocosms, respectively. These diffusive fluxes are always lower than those calculated for the nonbioturbated mesocosms (Fig. 3C). In all the control aquaria, Fe(II) concentrations increase rapidly and remain elevated with depth. We cannot directly compare between aquaria run under different levels of dissolved oxygen because the sediment was collected at different times of the year for each of the oxygen treatment aquaria pairs, and the basal levels of dissolved and solid phase iron differed between each experiment. Nonetheless, our calculations show that the bioturbated aquaria have a much lower potential for supplying Fe(II) to the overlying water column through diffusive flux compared to nonbioturbated aquaria.

Bioturbation and bioirrigation actively introduce oxygenated bottom water into reduced sediments, causing the biological and chemical oxidation of iron (Beam et al., 2018; Canfield, 1989). The surface sediment porewater Fe(II) is kept low in the bioturbated aquaria, which translates to the higher accumulation of poorly crystalline Fe(III)-oxides (Fig. 3). The accumulation of poorly crystalline Fe(III)-oxides was different between bioturbated and nonbioturbated aquaria with 108 and 48 μM oxygen, but not at 280 μM oxygen (Fig. 3). While the hydroxylamine hydrochloride extraction does not preserve the redox speciation of extracted iron minerals, it was shown to target ferrihydrite and lepidocrocite (Poulton and Canfield, 2005). Given that the hypoxic and suboxic bioturbated aquaria had greater amounts of poorly crystalline Fe than the non-bioturbated controls, but low diffusive fluxes suggest that there is another mechanism that brings the reduced fluid or Fe into contact with the oxygen. This is likely due to advective transport caused by *N. diversicolor* while it is irrigating its burrow. Finally, Fe(II) in the overlaying water was below the detection limit of the ferrozine assay (approximately 1 μM) under all conditions, indicating there was not a significant build-up of Fe(II), even under hypoxic conditions. While Fe (II) concentrations were below detection, we did observe that aquaria walls in the bioturbated mesocosms exhibited visible accumulation of Fe (III)-oxide-like precipitates compared to the controls (Supplementary Fig. 3). Visually it appeared the increasingly oxic mesocosms had greater accumulations. This indicates bioturbated mesocosms likely had increased amounts of dFe exported from the sediments to the water column, concurrent with other studies of benthic Fe flux (Elrod et al., 2004; Herbert et al., 2021). Some of this dFe may be in the form of chelated Fe(II) or Fe(III), and some may exist as very fine grained, hydrous Fe(III)-oxides as are known to be produced by Fe(II)-oxidizing Zetaproteobacteria that inhabit worm burrow walls (Beam et al., 2018; Toner et al., 2012).

Acid volatile sulfides are one pool of solid phase reduced iron and sulfur minerals, typically presenting in surface sediment as FeS, and result from the reaction between the reduced end products from sulfate and iron reduction (Liu et al., 2020). The profiles of AVS from paired bioturbated and control aquaria are similar and imply that the burial of reduced Fe and S was similar with and without *N. diversicolor*. FeS is oxidized abiotically by oxygen or biologically by microorganisms, thus bioturbation was expected to decrease the FeS content of bioturbated aquaria. This was not seen in the integrated AVS contents of the sediment, Fig. 3B. Thus, the net rate of FeS formation during the experimental time frame for all experiments was similar, with a lack of evidence for net loss or gain of FeS with or without worms. The ability of *N. diversicolor* to influence solid phase geochemistry appears to be limited to what intersects the burrow wall. The reoxidation of solid phase FeS, reintroduced to the oxic sediment through bioturbation is one mechanism that produces poorly-crystalline Fe(III)-oxides in marine sediments. There are no clear differences between bioturbated and non-bioturbated aquaria in FeS content at the end of the experiment, but there are increases in poorly-crystalline Fe(III)-oxides within the bioturbated aquaria at reduced oxygen concentration (Fig. 3A). This suggests that the diffusion of dissolved Fe(II), from either sulfide-mediated Fe(III)-oxide reduction or dissimilatory iron reduction (Michaud et al., 2020), across the oxic-anoxic boundaries created by worm burrows was

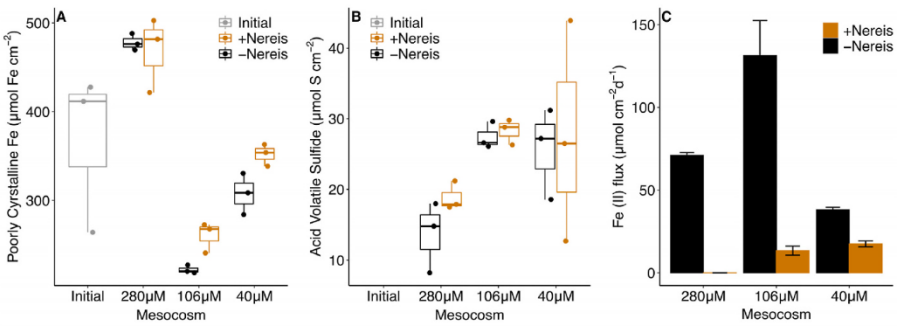

Fig. 3. Comparison of areal integrated poorly crystalline Fe over the top 10 cm (deepest sampled depth of all cores for poorly crystalline Fe analysis) of triplicate cores collected at the end of the experiment (A), and integrated acid volatile sulfide over the top 7 cm (deepest sampled depth of all cores for AVS analysis) of the triplicate cores collected at the end of the experiment (B). Poorly crystalline Fe was also quantified after sieving and before the experiment started, "initial material", and multiplied here by 10 cm assuming the sieved material was homogenized and to match the quantity of poorly crystalline Fe from the sampling over depth at the end of the experiment.

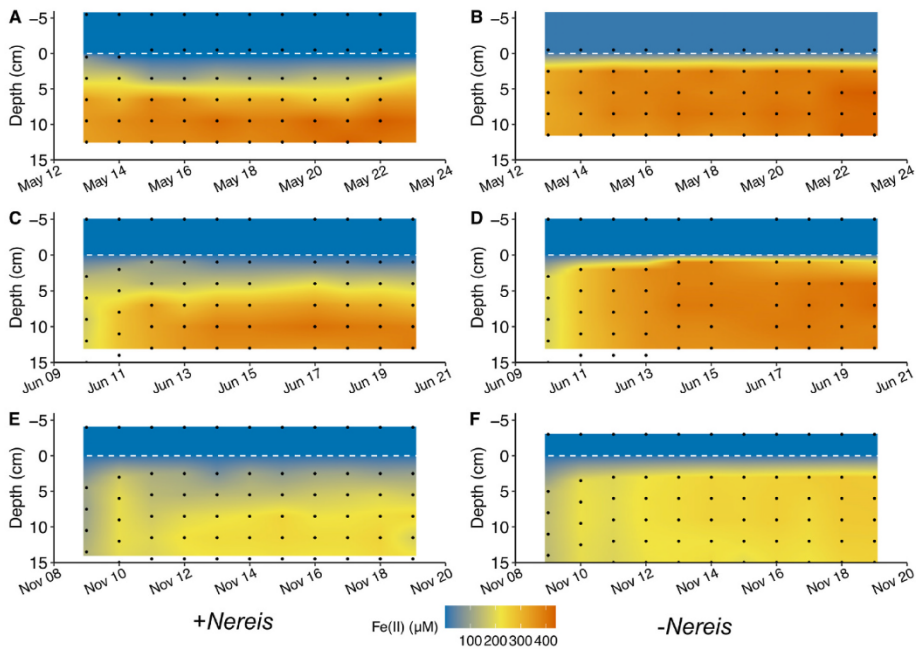

Fig. 4. Porewater Fe^{2+} concentrations in mesocosms that contained *Nereis diversicolor* (A, C, E) and did not contain *Nereis diversicolor* (B, D, F), with water column oxygen concentrations maintained at 280 μM (A, B), 106 μM (C, D), and 48 μM (E, F). The concentrations plotted are linear interpolations through the measured data points (black dots) and assuming a linear diffusive boundary layer that was equal in thickness (500 μm) across all the aquaria.

the source of iron responsible for producing the elevated levels of poorly-crystalline Fe(III)-oxides. While the diffusive flux across the 0 cm sediment-water interface is higher in nonbioturbated aquaria, this bulk measurement of flux does not take into account the more abundant redox interfaces created by burrowing worms that can increase the effective sediment-water surface area.

In comparison to another study, Thibault de Chanvalon et al. conducted fine scale 2-dimensional mapping of Fe(II) dynamics associated with *N. diversicolor* burrows that coupled mathematical modeling to a unique *in situ* device for visualizing Fe porewater gradients associated with worm burrows (Thibault de Chanvalon et al., 2017). Predictions from that work done under fully oxic conditons indicated reoxidation of Fe(II) associated with burrow walls consumed nearly 90% of the Fe flux, and that these oxides would be recycled 7–8 times before the Fe would either diffuse or be advected from the sediment. The fact we observed substantial Fe(III)-oxide accumulation associated with burrow walls at 280 μM O_2 is consistent with the work of Thibault de Chanvalon et al., and shows that under hypoxic conditions bioturbation still enhances the production of oxidized Fe over sediment without worms. Based on the greater accumulation of Fe(III)-oxides around burrow walls under fully oxic conditions compared to hypoxia, it is reasonable to assume the potential for Fe recycling decreases with increasing hypoxia. This, in turn, may affect the carbon cycle by limiting the capacity for organic carbon to be mineralized via dissimilatory Fe-reduction within sediments experiencing hypoxia, as Fe-reducing microorganisms preferentially use the less crystalline forms of Fe(III)-oxides (Laufer et al., 2020).

3.3. Microbial community analysis

Depth resolved microbial community analysis was conducted at 1, 3, 5, and 10 cm from both bioturbated and control aquaria for each O_2 condition at the termination of each experiment. With this intensity of sampling, we were unable to see notable differences between bioturbated and control aquaria within any of the experiments (Fig. 5); nor was there any depth stratification with respect to total community composition within the mesoscosms. The ecostates analysis indicated that the communities in the 48 and 106 μM O_2 treatments were a different ecostate (green bar in Fig. 5), than the community in the 280 μM treatment (blue bar in Fig. 5). This indicated the higher O_2 concentration in the overlaying water may have some impact on the microbial community in the sediment, although we cannot rule out the possibility that fundamental differences in the communities at the start of each experiment could have contributed to this difference in ecostate. A representative depth profile of the microbial community from this same mudflat site (Beam et al., 2020) had different ecostates from mesocosms presented here. Overall, these results indicate that mesocosm set up had a greater influence on microbial community composition than 10d of incubation at differing oxygen contents and worm presence.

A comparison of all the mesocosm OTUs, to all the OTUs previously analyzed from this same mudflat (Beam et al., 2020), revealed that 22 of the 25 most abundant OTUs were shared between these *in situ* collected samples and those collected at the end of the 10 d experiment (results not shown). Previous work has shown the abundance of Zetaproteobacteria, that catalyze lithotrophic Fe(II)-oxidation, are enriched in the Fe(III)-oxide encrustations on burrow walls where we assume they play an important role in microbially mediated Fe(II)-oxidation (Beam et al., 2020; McAllister et al., 2015). The relative abundance of Zetaproteobacteria tended to decrease with decreasing O_2 concentration in the mesocosms; however, differences between bioturbated and non-bioturbated conditions were not observed (Fig. 6A). The *Desulfobulbaceae* belong to a family of Deltaproteobacteria that includes a number of genera capable of diverse sulfur metabolisms, including sulfur disproportionation and sulfate reduction. *Desulfobulbaceae also* include the cable bacteria that can carry out long range electron transfer that link the oxidation of H_2S in sediments to the reduction of O_2 near the sediment-water interface (Kjeldsen et al., 2019; Nielsen et al., 2010; Ward et al., 2021). In each of the mesocosms, there was a general decrease in their relative abundance compared to the homogenized mud that was used to start the experiment (Fig. 6B). It is possible the physical disruption of the sediments for preparing the mesocosms may have interfered with metabolisms associated with the *Desulfobulbaceae* in undisturbed, natural sediments, for example the long-distance electron transfer of cable bacteria (Hermans et al., 2019; Malkin et al., 2014). One of the most abundant taxa in these sediments was the family *Desulfobacteraceae* that contains a number of known sulfate-reducing

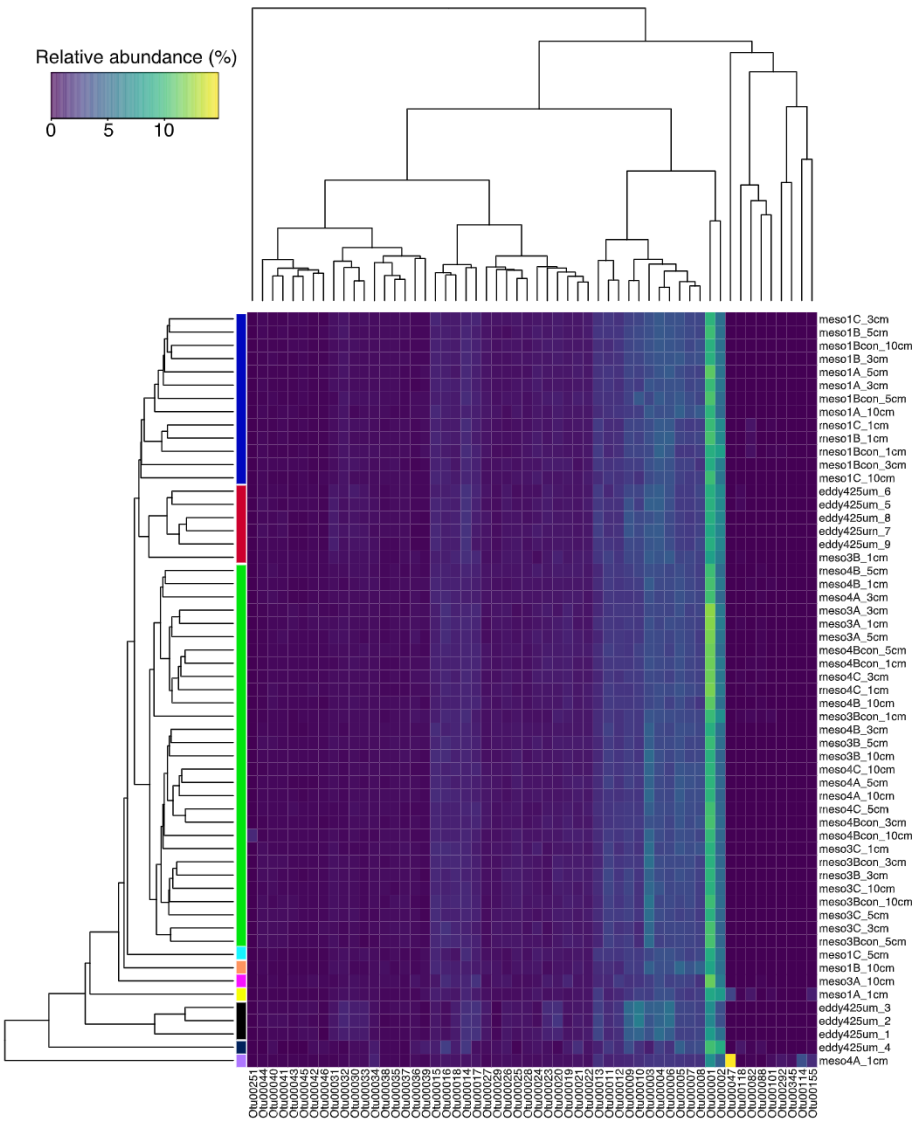

Fig. 5. Heatmap of OTU abundances for different treatments, and a core sample from the initial sediments at The Eddy with individual OTUs identified along the bottom, and sample identified on the right. Samples on the right are identified as "eddy" which is a core from The Eddy site taken as a representative sample of the sediments before worm and oxygen concentration manipulation in the mesocosms. The "meso" samples are those taken from after the 10 d of incubation at the different oxygen concentrations, where "meso1", "meso4", and "meso3" are the 280, 106, and 48 μM treatments, respectively. The "con" label (for control) represented sediments taken from mesocosms without *Nereis*. The numbers after the underscore in the label represent depths, in cm below the sediment surface. The ecostates analysis groups similar microbial communities together in the dendrogram shown on the left, and the vertical color bars highlight the nodes of the dendrogram that represent unique ecostates, a total of 10 different ecostates were identified. (For interpretation of the references to color in this figure legend, the reader is referred to the Web version of this article.)

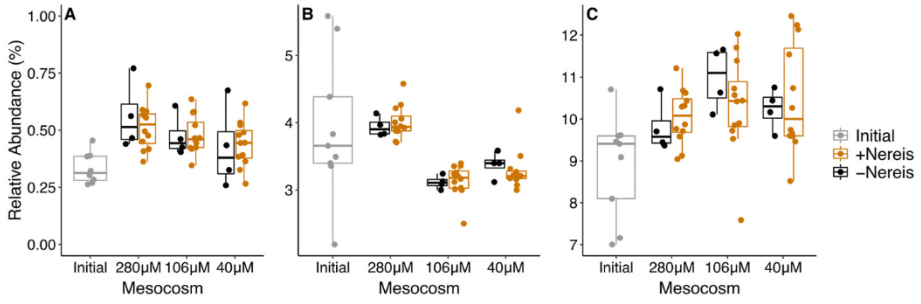

Fig. 6. Comparison of the sum of presumptive Fe(II)-oxidizing Zetaproteobacteria (*Mariprofundus*) and Betaproteobacteria (*Gallionella*) (A), Desulfobulbaceae, the family in which the Cable bacteria belong, (B), and Desulfobacteraceae (C) in initial Eddy mud samples and three mesocosms with and without *Nereis diversicolor*.

bacteria. Again, bioturbation did not seem to impact the relative abundances of this abundant functional group within mudflat sediments (Fig. 6C). The overall lack of discrimination in microbial populations between bioturbated and non-bioturbated mesocosms shows it was not possible to resolve differences in microbial community structure, although the presence of *N. diversicolor* clearly had an impact on sediment structure, and biogeochemical cycling of Fe. Our experimental design (10 d incubation) was not sufficient to observe growth of taxa that would respond to declines in oxygen saturation and redox interfaces caused by bioturbation. This is consistent with the findings of a recent study by Wyness et al. (2021) that found microbial community structure in another type of sediment mesocosm only showed significant changes after 70 weeks. There may have been changes in microbial communities associated with the burrow wall microenvironments, but that would only make up a small percentage of the bulk sediment, limiting the capacity to detect specific microbial responses to bioturbation.

4. Conclusions

The work presented here demonstrates that bioturbation and hypoxia have the potential to impact Fe-cycling in intertidal sediments. Non-bioturbated mesocosms had increased diffusive flux of Fe(II) across the sediment-water interface; however the bioturbated mesocosms accumulated greater amounts of reactive Fe(III)-oxides in association with burrow walls, indicating a greater potential for Fe-cycling, dFe flux, and Fe-mediated carbon cycling within the sediments. Implications from this work are that extreme hypoxia, defined here as ≤ 10 μM O_2 saturation of overlaying waters was not tolerated by *N. diversicolor*; however, high (40–50 μM O_2) and intermediate levels (~100 μM O_2) of hypoxia did not seem to impair the activity of these benthic invertebrates, but hypoxia did decrease the amount of reactive Fe(III)-oxides associated with burrow walls in the sediment. While microorganisms are important to Fe cycling, due to the short duration of these experiments, it was not possible to identify statistically significant changes in the present, but not active, benthic microbial community. This suggests measuring the biogeochemical response of sediments due to changes in bioturbation may be the most effective means of assessing the short-term impacts of changes in rates of bio-irrigation and bio-mixing on sediments. This study adds to the body of knowledge that bioturbation does play an important role in the Fe cycle of coastal marine sediments. Bioturbation enhances the iron cycle by producing more poorly crystalline Fe(III)-oxides in the sediment and an obvious, but unquantified source of dFe to the water column. As hypoxic conditions continue to expand in coastal sediments due to anthropogenic activities, our results indicate the production of poorly crystalline Fe(III)-oxides produced within surficial sediments due to bioturbation will decline, and impact sediment biogeochemical processes and Fe exchange with the water column.

CRediT authorship contribution statement

Jacob P. Beam: Methodology, Formal analysis, Data curation, Conceptualization. **Alexander B. Michaud:** Writing – review & editing, Writing – original draft, Formal analysis, Data curation. **David T. Johnston:** Writing – review & editing, Conceptualization. **Peter R. Girguis:** Writing – review & editing, Conceptualization. **David Emerson:** Conceptualization, Formal Analysis, Writing – original draft, Writing – review & editing.

Declaration of competing interest

The authors declare that they have no known competing financial interests or personal relationships that could have appeared to influence the work reported in this paper.

Data availability

Data will be made available on request.

Acknowledgements

We thank Sarabeth George for her help in sediment collection and preparation. This work was funded in part by National Science Foundation grant OCE-1459600 and DEB-1754358 to D. Emerson, with additional support for D. Emerson from NSF OIA-1849227. This material is also based upon support provided by the National Science Foundation (Grant No. NSF-OCE 1635365) and NASA awards 80NSSC19K1427 and 80NSSC18K1140 to P. Girguis.

Appendix A. Supplementary data

Supplementary data to this article can be found online at https://doi.org/10.1016/j.ecss.2022.108032.

References

Aller, R.C., Cochran, J.K., 2019. The critical role of bioturbation for particle dynamics, priming potential, and organic C remineralization in marine sediments: local and basin scales. Front. Earth Sci. 7, 1–14. https://doi.org/10.3389/feart.2019.00157.

Bartels-Hardege, H.D., Zeeck, E., 1990. Reproductive behaviour of Nereis diversicolor (Annelida: Polychaeta). Mar. Biol. 106, 409–412. https://doi.org/10.1007/BF01344320.

Beam, J.P., George, S., Record, N.R., Countway, P.D., Johnston, D.T., Girguis, P.R., Emerson, D., 2020. Mud, microbes, and macrofauna: seasonal dynamics of the iron biogeochemical cycle in an intertidal mudflat. Front. Mar. Sci. 7, 1–16. https://doi.org/10.3389/fmars.2020.562617.

Beam, J.P., Scott, J.J., McAllister, S.M., Chan, C.S., McManus, J., Meysman, F.J.R., Emerson, D., 2018. Biological rejuvenation of iron oxides in bioturbated marine sediments. ISME J. 12, 1389–1394. https://doi.org/10.1038/s41396-017-0032-6.

Bianchi, T.S., Aller, R.C., Atwood, T.B., Brown, C.J., Buatois, L.A., Levin, L.A., Levinton, J.S., Middelburg, J.J., Morrison, E.S., Regnier, P., Shields, M.R., Snelgrove, P.V.R., Sotka, E.E., Stanley, R.R.E., 2021. What global biogeochemical consequences will marine animal-sediment interactions have during climate change? Elementa 9, 1–25. https://doi.org/10.1525/elementa.2020.00180.

Birchill, A.J., Hartner, N.T., Kunde, K., Siemering, B., Daniels, C., González-Santana, D., Milne, A., Ussher, S.J., Worsfold, P.J., Leopold, K., Painter, S.C., Lohan, M.C., 2019. The eastern extent of seasonal iron limitation in the high latitude North Atlantic Ocean. Sci. Rep. 9, 1–12. https://doi.org/10.1038/s41598-018-37436-3.

Broecker, W.S., Peng, T.-H., 1974. Gas exchange rates between air and sea. Tellus 26, 21–35.

Buongiorno, J., Herbert, L.C., Wehrmann, L.M., Michaud, A.B., Laufer, K., Røy, H., Jørgensen, B.B., Szynkiewicz, A., Faiia, A., Yeager, K.M., Schindler, K., Lloyd, K.G., 2019. Complex microbial communities drive iron and sulfur cycling in arctic fjord sediments. Appl. Environ. Microbiol. 85 https://doi.org/10.1128/AEM.00949-19 e00949-19.

Butterfield, N.J., 2018. Oxygen, animals and aquatic bioturbation: an updated account. Geobiology 16, 3–16. https://doi.org/10.1111/gbi.12267.

Canfield, D.E., 1989. Reactive iron in marine sediments. 1989. Geochem. Cosmochim. Acta. 53, 619–632.

Cline, J.D., 1969. Spectrophotometric determination of hydrogen sulfide in natural waters. Limnol. Oceanogr. 14, 454–458. https://doi.org/10.4319/lo.1969.14.3.0454.

Dale, A.W., Nickelsen, L., Scholz, F., Hensen, C., Oschlies, A., Wallmann, K., 2015. A revised global estimate of dissolved iron fluxes from marine sediments. Global Biogeochem. Cycles 29, 691–707. https://doi.org/10.1002/2014GB005017.

Davey, J.T., 1994. The architecture of the burrow of Nereis diversicolor and its quantification in relation to sediment-water exchange. J. Exp. Mar. Biol. Ecol. 179, 115–129. https://doi.org/10.1016/0022-0981(94)90020-5.

Dorgan, K.M., Jumars, P.A., Johnson, B., Boudreau, B.P., Landis, E., 2005. Burrowing mechanics: burrow extension by crack propagation. Nature 433, 2005.

Elrod, V.A., Berelson, W.M., Coale, K.H., Johnson, K.S., 2004. The flux of iron from continental shelf sediments: a missing source for global budgets. Geophys. Res. Lett. 31, 2–5. https://doi.org/10.1029/2004GL020216.

Fennel, K., Testa, J.M., 2019. Biogeochemical controls on coastal hypoxia. Ann. Rev. Mar. Sci 11, 105–130. https://doi.org/10.1146/annurev-marine-010318-095138.

Forster, S., Graf, G., Kitlar, J., Powilleit, M., 1995. Effects of bioturbation in oxic and hypoxic conditions: a microcosm experiment with a North Sea sediment community. Mar. Ecol. Prog. Ser. 116, 153–162. https://doi.org/10.3354/meps116153.

Fossing, H., Jørgensen, B.B., 1989. Measurement of bacterial sulfate reduction in sediments: evaluation of a single-step chromium reduction method. Biogeochemistry 8, 205–222. https://doi.org/10.1007/BF00002889.

Gribsholt, B., Kostka, J.E., Kristensen, E., 2003. Impact of fiddler crabs and plant roots on sediment biogeochemistry in a Georgia saltmarsh. Mar. Ecol. Prog. Ser. 259, 237–251. https://doi.org/10.3354/meps259237.

Herbert, L.C., Michaud, A.B., Laufer-Meiser, K., Hoppe, C.J.M., Zhu, Q., Aller, R.C., Jørgensen, B.B., Wehrmann, L.M., 2022. Tight benthic-pelagic coupling drives seasonal and interannual changes in iron-sulfur cycling in Arctic fjord sediments (Kongsfjorden, Svalbard). J. Mar. Syst. 225 https://doi.org/10.1016/j.jmarsys.2021.103645.

Herbert, L.C., Zhu, Q., Michaud, A.B., Laufer-Meiser, K., Jones, C.K., Riedinger, N., Stooksbury, Z.S., Aller, R.C., Jørgensen, B.B., Wehrmann, L.M., 2021. Benthic iron flux influenced by climate-sensitive interplay between organic carbon availability and sedimentation rate in Arctic fjords. Limnol. Oceanogr. 66, 3374–3392. https://doi.org/10.1002/lno.11885.

Hermans, M., Lenstra, W.K., Hidalgo-Martinez, S., Van Helmond, N.A.G.M., Witbaard, R., Meysman, F.J.R., Gonzalez, S., Slomp, C.P., 2019. Abundance and biogeochemical impact of cable bacteria in Baltic Sea sediments. Environ. Sci. Technol. 53, 7494–7503. https://doi.org/10.1021/acs.est.9b01665.

Homoky, W.B., Severmann, S., McManus, J., Berelson, W.M., Riedel, T.E., Statham, P.J., Mills, R.A., 2012. Dissolved oxygen and suspended particles regulate the benthic flux of iron from continental margins. Mar. Chem. 134–135, 59–70. https://doi.org/10.1016/j.marchem.2012.03.003.

Jessen, G.L., Lichtschlag, A., Ramette, A., Pantoja, S., Rossel, P.E., Schubert, C.J., Struck, U., Boetius, A., 2017. Hypoxia causes preservation of labile organic matter and changes seafloor microbial community composition (Black Sea). Sci. Adv. 3 https://doi.org/10.1126/sciadv.1601897.

Jørgensen, B.B., Des Marais, D.J., 1990. The diffusive boundary layer of sediments: oxygen microgradients over a microbial mat. Limnol. Oceanogr. 35, 1343–1355.

Kjeldsen, K.U., Schreiber, L., Thorup, C.A., Boesen, T., Bjerg, J.T., Yang, T., Dueholm, M. S., Larsen, S., Risgaard-Petersen, N., Nierychlo, M., Schmid, M., Bøggild, A., de

Vossenberg, J. van, Geelhoed, J.S., Meysman, F.J.R., Wagner, M., Nielsen, P.H., Nielsen, L.P., Schramm, A., 2019. On the evolution and physiology of cable bacteria. Proc. Natl. Acad. Sci. U.S.A. 116, 19116–19125. https://doi.org/10.1073/pnas.1903514116.

Kozich, J.J., Westcott, S.L., Baxter, N.T., Highlander, S.K., Schloss, P.D., 2013. Development of a dual-index sequencing strategy and curation pipeline for analyzing amplicon sequence data on the miseq illumina sequencing platform. Appl. Environ. Microbiol. 79, 5112–5120. https://doi.org/10.1128/AEM.01043-13.

Kristensen, E., Kostka, J.E., 2013. Macrofaunal burrows and irrigation in marine sediment: microbiological and biogeochemical interactions. Interact. Between macro- microorg. Marit. Sediments 125–157. https://doi.org/10.1029/CE060p0125.

Laufer-Meiser, K., Michaud, A.B., Maisch, M., Byrne, J.M., Kappler, A., Patterson, M.O., Røy, H., Jørgensen, B.B., 2021. Potentially bioavailable iron produced through benthic cycling in glaciated Arctic fjords of Svalbard. Nat. Commun. 12, 1–13. https://doi.org/10.1038/s41467-021-21558-w.

Laufer, K., Michaud, A.B., Røy, H., Jørgensen, B.B., 2020. Reactivity of iron minerals in the seabed toward microbial reduction – a comparison of different extraction techniques. Geomicrobiol. J. 37, 170–189. https://doi.org/10.1080/01490451.2019.1679291.

Laufer, K., Røy, H., Jørgensen, B.B., Kappler, A., 2016. Evidence for the existence of autotrophic nitrate-reducing Fe(II)-oxidizing bacteria in marine coastal sediment. Appl. Environ. Microbiol. 82, 6120–6131. https://doi.org/10.1128/AEM.01570-16.

Lenstra, W.K., Hermans, M., Séguret, M.J.M., Witbaard, R., Behrends, T., Dijkstra, N., van Helmond, N.A.G.M., Kraal, P., Laan, P., Rijkenberg, M.J.A., Severmann, S., Teacă, A., Slomp, C.P., 2019. The shelf-to-basin iron shuttle in the Black Sea revisited. Chem. Geol. 511, 314–341. https://doi.org/10.1016/j.chemgeo.2018.10.024.

Liu, J., Pellerin, A., Antler, G., Kasten, S., Findlay, A.J., Dohrmann, I., Røy, H., Turchyn, A.V., Jørgensen, B.B., 2020. Early diagenesis of iron and sulfur in Bornholm Basin sediments: the role of near-surface pyrite formation. Geochem. Cosmochim. Acta 284, 43–60. https://doi.org/10.1016/j.gca.2020.06.003.

Malkin, S.Y., Rao, A.M.F., Seitaj, D., Vasquez-Cardenas, D., Zetsche, E.M., Hidalgo-Martinez, S., Boschker, H.T.S., Meysman, F.J.R., 2014. Natural occurrence of microbial sulphur oxidation by long-range electron transport in the seafloor. ISME J. 8, 1843–1854. https://doi.org/10.1038/ismej.2014.41.

Martin, J.H., Fitzwater, S.E., Gordon, R.M., 1990. Iron deficiency limits phytoplankton growth in Antarctic waters. Global Biogeochem. Cycles 4, 5–12.

McAllister, S.M., Barnett, J.M., Heiss, J.W., Findlay, A.J., MacDonald, D.J., Dow, C.L., Luther, G.W., Michael, H.A., Chan, C.S., 2015. Dynamic hydrologic and biogeochemical processes drive microbially enhanced iron and sulfur cycling within the intertidal mixing zone of a beach aquifer. Limnol. Oceanogr. 60, 329–345. https://doi.org/10.1111/lno.10029.

Meysman, F.J.R., Galaktionov, O.S., Gribsholt, B., Middelburg, J.J., 2006a. Bioirrigation in permeable sediments: advective pore-water transport induced by burrow ventilation. Limnol. Oceanogr. 51, 142–156. https://doi.org/10.4319/lo.2006.51.1.0142.

Meysman, F.J.R., Middelburg, J.J., Heip, C.H.R., 2006b. Bioturbation: a fresh look at Darwin's last idea. Trends Ecol. Evol. 21, 688–695. https://doi.org/10.1016/j.tree.2006.08.002.

Michaud, A.B., Laufer, K., Findlay, A., Pellerin, A., Antler, G., Turchyn, A.V., Røy, H., Wehrmann, L.M., Jørgensen, B.B., 2020. Glacial influence on the iron and sulfur cycles in Arctic fjord sediments (Svalbard). Geochem. Cosmochim. Acta 280, 423–440. https://doi.org/10.1016/j.gca.2019.12.033.

Nielsen, L.P., Risgaard-Petersen, N., Fossing, H., Christensen, P.B., Sayama, M., 2010. Electric currents couple spatially separated biogeochemical processes in marine sediment. Nature 463, 1071–1074. https://doi.org/10.1038/nature08790.

O'Brien, J., Record, N., Countway, P., 2016. The power and pitfalls of Dirichlet-multinomial mixture models for ecological count data. bioRxiv. https://doi.org/10.1101/045468.

Oksanen, J., Blanchet, F.G., Kindt, P., Legendre, P., Minchin, P.R., O'Hara, R.B., Simpson, G.L., Solymos, P., Henry, M., Stevens, H., Wagner, H., 2013. Vegan: community ecology package. R Packag 2, 0-10.

Otte, J.M., Blackwell, N., Ruser, R., Kappler, A., Kleindienst, S., Schmidt, C., 2019. N_2O formation by nitrite-induced (chemo)denitrification in coastal marine sediment. Sci. Rep. 9, 10691 https://doi.org/10.1038/s41598-019-47172-x.

Pischedda, L., Cuny, P., Esteves, J.L., Poggiale, J.C., Gilbert, F., 2012. Spatial oxygen heterogeneity in a *Hediste diversicolor* irrigated burrow. Hydrobiologia 680, 109–124. https://doi.org/10.1007/s10750-011-0907-x.

Poulton, S., Canfield, D.E., 2005. Development of a sequential extraction procedure for iron: implications for iron partitioning in continentally derived particulates. Chem. Geol. 214, 209–221. https://doi.org/10.1016/j.chemgeo.2004.09.003.

R Core Team, 2020. R: A Language and Environment for Statistical Computing.

Raiswell, R., Canfield, D.E., 2012. Iron export by icebergs and subglacial runoff. Geochemical Perspect 1, 72–80.

Record, N.R., O'Brien, J.D., Stamieszkin, K., Runge, J.A., 2017. Omic-Style statistical clustering reveals old and new patterns in the gulf of Maine ecosystem. Can. J. Fish. Aquat. Sci. 74, 1061–1076. https://doi.org/10.1139/cjfas-2016-0151.

Røy, H., Weber, H.S., Tarpgaard, I.H., Ferdelman, T.G., Jørgensen, B.B., 2014. Determination of dissimilatory sulfate reduction rates in marine sediment via radioactive 35S tracer. Limnol Oceanogr. Methods 12, 196–211. https://doi.org/10.4319/lom.2014.12.196.

Schloss, P.D., Westcott, S.L., Ryabin, T., Hall, J.R., Hartmann, M., Hollister, E.B., Lesniewski, R.A., Oakley, B.B., Parks, D.H., Robinson, C.J., Sahl, J.W., Stres, B., Thallinger, G.G., Van Horn, D.J., Weber, C.F., 2009. Introducing mothur: open-source, platform-independent, community-supported software for describing and comparing microbial communities. Appl. Environ. Microbiol. 75, 7537–7541. https://doi.org/10.1128/AEM.01541-09.

Schneider, C.A., Rasband, W.S., Eliceiri, K.W., 2012. NIH Image to ImageJ: 25 years of image analysis. Nat. Methods 9, 671–675. https://doi.org/10.1038/nmeth.2089.

Schöttler, U., 1979. On the anaerobic metabolism of three species of *Nereis* (Annelida). Mar. Ecol. Prog. Ser. 1, 249–254. https://doi.org/10.3354/meps001249.

Scott, J.J., Glazer, B.T., Emerson, D., 2017. Bringing microbial diversity into focus: high-resolution analysis of iron mats from the Lō'ihi Seamount. Environ. Microbiol. 19, 301–316. https://doi.org/10.4324/9781315830094-2.

Severmann, S., McManus, J., Berelson, W.M., Hammond, D.E., 2010. The continental shelf benthic iron flux and its isotope composition. Geochem. Cosmochim. Acta 74, 3984–4004. https://doi.org/10.1016/j.gca.2010.04.022.

Stookey, L.L., 1970. Ferrozine - a new spectrophotometric reagent for iron. Anal. Chem. 43, 779–781.

Tagliabue, A., Bowie, A.R., Boyd, P.W., Buck, K.N., Johnson, K.S., Saito, M.A., 2017. The integral role of iron in ocean biogeochemistry. Nature 543, 51–59. https://doi.org/10.1038/nature21058.

Thibault de Chanvalon, A., Metzger, E., Mouret, A., Knoery, J., Geslin, E., Meysman, F.J.R., 2017. Two dimensional mapping of iron release in marine sediments at submillimetre scale. Mar. Chem. 191, 34–49. https://doi.org/10.1016/j.marchem.2016.04.003.

Toner, B.M., Berquó, T.S., Michel, F.M., Sorensen, J.V., Templeton, A.S., Edwards, K.J., 2012. Mineralogy of iron microbial mats from Loihi Seamount. Front. Microbiol. 3, 1–18. https://doi.org/10.3389/fmicb.2012.00118.

van de Velde, S.J., Hülse, D., Reinhard, C.T., Ridgwell, A., 2021. Iron and sulfur cycling in the cGENIE.muffin Earth system model (v0.9.21). Geosci. Model Dev. (GMD) 14, 2713–2745. https://doi.org/10.5194/gmd-14-2713-2021.

van de Velde, S., Meysman, F.J.R., 2016. The influence of bioturbation on iron and sulphur cycling in marine sediments: a model analysis. Aquat. Geochem. 22, 469–504. https://doi.org/10.1007/s10498-016-9301-7.

van de Velde, S.J., Hidalgo-Martinez, S., Callebaut, I., Antler, G., James, R.K., Leermakers, M., Meysman, F.J.R., 2020. Burrowing fauna mediate alternative stable states in the redox cycling of salt marsh sediments. Geochem. Cosmochim. Acta 276, 31–49. https://doi.org/10.1016/j.gca.2020.02.021.

Ward, L.M., Bertran, E., Johnston, D.T., 2021. Expanded genomic sampling refines current understanding of the distribution and evolution of sulfur metabolisms in the desulfobulbales. Front. Microbiol. 12 https://doi.org/10.3389/fmicb.2021.666052.

Wyness, A.J., Fortune, I., Blight, A.J., Browne, P., Hartley, M., Holden, M., Paterson, D. M., 2021. Ecosystem engineers drive differing microbial community composition in intertidal estuarine sediments. PLoS One 16, 1–20. https://doi.org/10.1371/journal.pone.0240952.

Yarza, P., Yilmaz, P., Pruesse, E., Glöckner, F.O., Ludwig, W., Schleifer, K.H., Whitman, W.B., Euzéby, J., Amann, R., Rosselló-Móra, R., 2014. Uniting the classification of cultured and uncultured bacteria and archaea using 16S rRNA gene sequences. Nat. Rev. Microbiol. 12, 635–645. https://doi.org/10.1038/nrmicro3330.